First published in Inverse Problems and Imaging in Vol. 2, No. 3, 2008,
published by the American Institute of Mathematical Sciences

Inverse Problems and Imaging
Volume 2, No. 3, 2008, 355–372

Web site: http://www.aimSciences.org

FACTORIZATION METHOD AND INCLUSIONS OF MIXED TYPE IN AN INVERSE ELLIPTIC BOUNDARY VALUE PROBLEM

Bastian Gebauer

Institut für Mathematik
Johannes Gutenberg-Universität Mainz
55099 Mainz, Germany

Nuutti Hyvönen

Institute of Mathematics
Helsinki University of Technology
FI-02015 HUT, Finland

(Communicated by Andreas Kirsch)

Abstract. In various imaging problems the task is to use the Cauchy data of the solutions to an elliptic boundary value problem to reconstruct the coefficients of the corresponding partial differential equation. Often the examined object has known background properties but is contaminated by inhomogeneities that cause perturbations of the coefficient functions. The factorization method of Kirsch provides a tool for locating such inclusions. In this paper, the factorization technique is studied in the framework of coercive elliptic partial differential equations of the divergence type: Earlier it has been demonstrated that the factorization algorithm can reconstruct the support of a strictly positive (or negative) definite perturbation of the leading order coefficient, or if that remains unperturbed, the support of a strictly positive (or negative) perturbation of the zeroth order coefficient. In this work we show that these two types of inhomogeneities can, in fact, be located simultaneously. Unlike in the earlier articles on the factorization method, our inclusions may have disconnected complements and we also weaken some other a priori assumptions of the method. Our theoretical findings are complemented by two-dimensional numerical experiments that are presented in the framework of the diffusion approximation of optical tomography.

1. **Introduction.**

Let us consider the following inverse boundary value problem: Determine the *diffusion tensor* $\sigma(x) > 0$ and the *absorption coefficient* $\mu(x) > 0$ in the elliptic equation

$$\nabla \cdot \sigma \nabla u - \mu u = 0 \quad \text{in } \Omega \tag{1}$$

when all possible pairs of Neumann and Dirichlet boundary values of u are measured on $\partial\Omega$. This problem arises, e.g., in optical tomography, cf. Arridge [1] and Heino and Somersalo [14], if the measurements are static in time and modelled by the diffusion approximation of the radiative transfer equation.

2000 *Mathematics Subject Classification.* Primary: 35R30; Secondary: 65N21.
Key words and phrases. Factorization method, inverse elliptic boundary value problems, inclusions.

If μ is known to be identically zero, (1) transforms into the conductivity equation, for which the isotropic inverse boundary value problem is known to be uniquely solvable under suitable dimension-dependent smoothness conditions on the scalar valued function σ; see Astala and Päivärinta [3], Nachman [22], Sylvester and Uhlmann [23], and the references therein. However, if $\mu > 0$, it can be shown that the coefficients of (1) cannot, in general, be uniquely determined from the knowledge of the Neumann-to-Dirichlet boundary map even if σ is scalar valued, cf. Arridge and Lionheart [2]. In this work, we consider a simplified yet practical version of this inverse boundary value problem with emphasis on obtaining a constructive algorithm.

Various imaging problems of practical importance consider locating inhomogeneities inside objects with known background properties. For example, detection of cracks and air bubbles in some building material and distinguishing cancerous tissue from healthy background fall into this category of problems. The factorization method of Kirsch [19], introduced originally within inverse obstacle scattering, provides a tool that can be applied to these kinds of situations in the framework of diffuse tomography methods [11]. The theoretical aspects and the numerical implementation of the technique for the inverse conductivity problem have been considered, e.g., by Brühl in [6], by the authors in [12] and in the works of Brühl and Hanke [5, 13], respectively. The generalization to the case of more general equations of the type (1) has been tackled by Kirsch in [20] and by the authors in [11, 15, 16], of which the first two references provide more general analysis whereas the latter two concentrate more specifically on optical tomography.

Although the factorization method has already been studied quite extensively with the elliptic equation (1), simultaneous characterization of absorbing and diffuse inhomogeneities is yet to be considered: In [11, 15, 20] the aim is to find the support of a strictly positive (or negative) perturbation of σ; the possible variation in μ is only treated as a nuisance causing a compact perturbation that may sometimes result in the failure of the method. On the other hand, [16] considers only the case where μ is perturbed but σ is not. Moreover, no previous work on the factorization method investigates the situation where the inhomogeneity, i.e., the union of the supports of the perturbations, does not have a connected complement and this is also the first paper where the supports of the two perturbations need not be related in any manner.

Assume that the perturbations of σ and μ are positive (or negative) semi definite. In this work, we show that the factorization method distinguishes between points of the following two types: (a) Such $x \in \Omega$ that one cannot travel from x to $\partial\Omega$ without climbing over a strictly positive (or negative) hump caused by *either* the perturbation of σ *or* that of μ. (b) $x \in \Omega$ for which there exists an open neighbourhood $U \subset \Omega$ of the boundary $\partial\Omega$ so that $x \in U$ and U intersects *neither* the support of the perturbation of σ *nor* that of the perturbation of μ. This statement is made unambiguous in Theorem 2.3 below. In particular, we want to emphasize that we do not pose any regularity conditions on the perturbations of σ and μ and do not ask for any special behaviour at the boundaries of the perturbation supports as the authors do in the references we have cited above (apart from [12]). Our theoretical findings are complemented by two-dimensional numerical experiments.

This text is organized as follows. In section 2, we introduce our framework, state the characterization result and present its proof. Section 3 verifies the theoretical results numerically and Section 4 contains the concluding remarks.

2. **Characterization of inclusions of mixed type.** Let $\Omega \subset \mathbb{R}^n$, $n \geq 2$, be a smooth, bounded domain, $\sigma : \Omega \to \mathbb{R}^{n\times n}$ a symmetric diffusion tensor and $\mu : \Omega \to \mathbb{R}$ an absorption coefficient. The elliptic boundary value problem we are interested in is as follows: For the input $f \in L^2(\partial\Omega)$, find the weak solution $u \in H^1(\Omega)$ of

$$\nabla \cdot \sigma \nabla u - \mu u = 0 \quad \text{in } \Omega, \quad \nu \cdot \sigma \nabla u = f \quad \text{on } \partial\Omega, \tag{2}$$

where ν is the exterior unit normal of $\partial\Omega$. If $\sigma \in L^\infty(\Omega, \mathbb{R}^{n\times n})$ and $\mu \in L^\infty(\Omega, \mathbb{R})$ satisfy the estimates

$$\sigma \geq c_\sigma I > 0, \quad \mu \geq c_\mu > 0, \quad c_\sigma, c_\mu \in \mathbb{R}_+, \tag{3}$$

the forward problem (2) has a unique solution that depends linearly and continuously on the input f. Here and in the following, we use "$>$" in the sense of positive definiteness almost everywhere in Ω.

When solving the inverse boundary value problem corresponding to (2), one tries to reconstruct the coefficients σ and μ from the knowledge of the Neumann-to-Dirichlet map

$$\Lambda_\sigma : f \mapsto u|_{\partial\Omega}, \quad L^2(\partial\Omega) \to L^2(\partial\Omega),$$

which is linear, compact and self-adjoint and can also be considered as an isomorphism from $H^{-1/2}(\partial\Omega)$ to $H^{1/2}(\partial\Omega)$.

2.1. **The main result.** In this work, we assume that the coefficients of (2) are of the form

$$\sigma = \sigma_0 I + \kappa, \quad \mu = \mu_0 + \eta, \tag{4}$$

where $\sigma_0, \mu_0 > 0$ are the known constant background diffusion and absorption coefficients, respectively, and the perturbations $\kappa \in L_c^\infty(\Omega, \mathbb{R}^{n\times n})$ and $\eta \in L_c^\infty(\Omega, \mathbb{R})$ are assumed to be such that σ is symmetric and (3) is satisfied. Here L_c^∞ denotes the space of L^∞-functions whose supports are compact subsets of Ω. Take note that the results presented below would remain valid if the constant and isotropic background values in (4) were replaced by any other a priori known background coefficients that satisfy (3) and enable unique continuation of Cauchy data from $\partial\Omega$ to the interior of Ω. The same comment applies to the smoothness of the boundary $\partial\Omega$, as well.

In what follows, we will denote the Neumann-to-Dirichlet boundary map corresponding to the perturbed coefficients σ and μ by Λ and the map corresponding to the background coefficients σ_0 and μ_0 by Λ_0. Our goal is to obtain constructive information on the supports of κ and η via boundary measurements by looking at the range of the square root of $|\Lambda_0 - \Lambda|$. Notice that Λ_0 can be computed and Λ can, in principle, be measured. The techniques applied here stem from the works of Kirsch [19] and Brühl [6] and they have been used with elliptic equations of the type (2) in the works of Bal [4], Kirsch [20] and the authors [11, 15, 16, 18], as well.

Before presenting our characterization results, let us define two auxiliary concepts. To motivate the first definition, recall that the support of a locally integrable function f is the complement of the set of all points that have an open neighbourhood in which f vanishes almost everywhere. In [21], Kusiak and Sylvester introduced the so-called *infinity support* of f by taking the complement of the smaller set of points that have an *unbounded* open neighbourhood with this property. Thus, roughly speaking, the infinity support is the union of the support with all points that cannot be connected to infinity without crossing the support. We introduce now the analogous concept with infinity replaced by the boundary $\partial\Omega$. Here and in the following, we denote by $\|\cdot\|_2$ the matrix norm corresponding to the Euclidean vector norm.

Definition 2.1. The $\partial\Omega$-*support* of $g \in L^1_{\mathrm{loc}}(\Omega, \mathbb{R}^{d\times d})$ is the complement of the set of all $x \in \Omega$ for which there exists a (relatively) open $U \subset \overline{\Omega}$ with $x \in U$, $\partial\Omega \cap U \neq \emptyset$, and $g|_U$ vanishes almost everywhere. We denote this set by $\mathrm{supp}_{\partial\Omega}\, g$.

The *combined* $\partial\Omega$-*support* $\mathrm{supp}_{\partial\Omega}\,(g_1, g_2)$ of $g_1 \in L^1_{\mathrm{loc}}(\Omega, \mathbb{R}^{d_1\times d_1})$ and $g_2 \in L^1_{\mathrm{loc}}(\Omega, \mathbb{R}^{d_2\times d_2})$ is defined by

$$\mathrm{supp}_{\partial\Omega}\,(g_1, g_2) := \mathrm{supp}_{\partial\Omega}(\|g_1\|_2 + \|g_2\|_2).$$

Definition 2.2. A point $y \in \Omega$ is *shaded* by the symmetric tensors $g_1 \in L^\infty_c(\Omega, \mathbb{R}^{d_1\times d_1})$ and $g_2 \in L^\infty_c(\Omega, \mathbb{R}^{d_2\times d_2})$ if there exists a smooth domain $D \subset \Omega$, with $\overline{D} \subset \Omega$ and $\Omega \setminus \overline{D}$ connected, such that $y \in D$ and for each $z \in \partial D$ there exist constants $\epsilon_z, r_z > 0$ such that

$$|g_j| > \epsilon_z I \quad \text{almost everywhere in } B(z, r_z)$$

for $j = 1$ or $j = 2$. Here $B(z, r_z)$ denotes the open ball of radius r_z centered at z. The set of all points shaded by g_1 and g_2 is denoted by $\mathrm{sh}(g_1, g_2)$.

Take note that $\mathrm{supp}_{\partial\Omega}\,(g_1, g_2)$ is closed and consists of the supports of g_1 and g_2 together with the holes that cannot be connected to $\partial\Omega$ without crossing the support of g_1 or that of g_2. On the other hand, $\mathrm{sh}(g_1, g_2)$ is open and contains $x \in \Omega$ if one cannot travel from x to the boundary $\partial\Omega$ without going over a strictly positive hump in $|g_1|$ or in $|g_2|$. In particular, $\mathrm{sh}(g_1, g_2) \subseteq \mathrm{int}(\mathrm{supp}_{\partial\Omega}\,(g_1, g_2))$ but the inclusion does not need to hold in the other direction.

Finally, let us introduce a singular solution for scanning the object Ω: Fix $y \in \Omega$ and consider the solution $\Phi_y \in C^\infty(\overline{\Omega}\setminus\{y\})$ of the following homogeneous Neumann problem

$$\sigma_0 \Delta\Phi_y(x) - \mu_0 \Phi_y(x) = \delta(x - y) \quad \text{for } x \in \Omega, \quad \sigma_0 \frac{\partial \Phi_y}{\partial \nu} = 0 \quad \text{on } \partial\Omega, \tag{5}$$

where δ is the delta functional. Notice that Φ_y can be computed without any information on κ and η. Our main result is as follows:

Theorem 2.3. *Assume that either $\kappa, \eta \geq 0$ or $\kappa, \eta \leq 0$. If $y \in \mathrm{sh}(\kappa, \eta)$, the boundary value $\Phi_y|_{\partial\Omega}$ belongs to the range of $|\Lambda_0 - \Lambda|^{1/2}$. Conversely, $\Phi_y|_{\partial\Omega}$ is not included in the range of $|\Lambda_0 - \Lambda|^{1/2}$ if $y \notin \mathrm{supp}_{\partial\Omega}\,(\kappa, \eta)$.*

Theorem 2.3 is arguably a little difficult to comprehend. In consequence, we present five examples that demonstrate its strength but also its slight shortcomings. In all examples $\Omega \subset \mathbb{R}^2$ is the unit disk and the perturbations of the first four examples are visualized in Figure 1: κ is strictly positive definite in the regions filled by horizontal lines and zero elsewhere; η is strictly positive in the regions filled by vertical lines and zero elsewhere.

Example 2.1. Consider the inclusion geometry visualized in the top left image of Figure 1. According to Theorem 2.3, the test function $\Phi_y|_{\partial\Omega}$ belongs to the range of $|\Lambda_0 - \Lambda|^{1/2}$ if y lies in either of the two open disks marked by the thick solid line. On the other hand, if y belongs to the complement of the closure of these disks, $\Phi_y|_{\partial\Omega}$ is not in the range of $|\Lambda_0 - \Lambda|^{1/2}$. □

Example 2.2. Assume that the inhomogeneities inside Ω are given by the top right image of Figure 1. Theorem 2.3 tells us that $\Phi_y|_{\partial\Omega}$ belongs to the range of $|\Lambda_0 - \Lambda|^{1/2}$ if y lies in one of the three open squares marked by the thick solid line

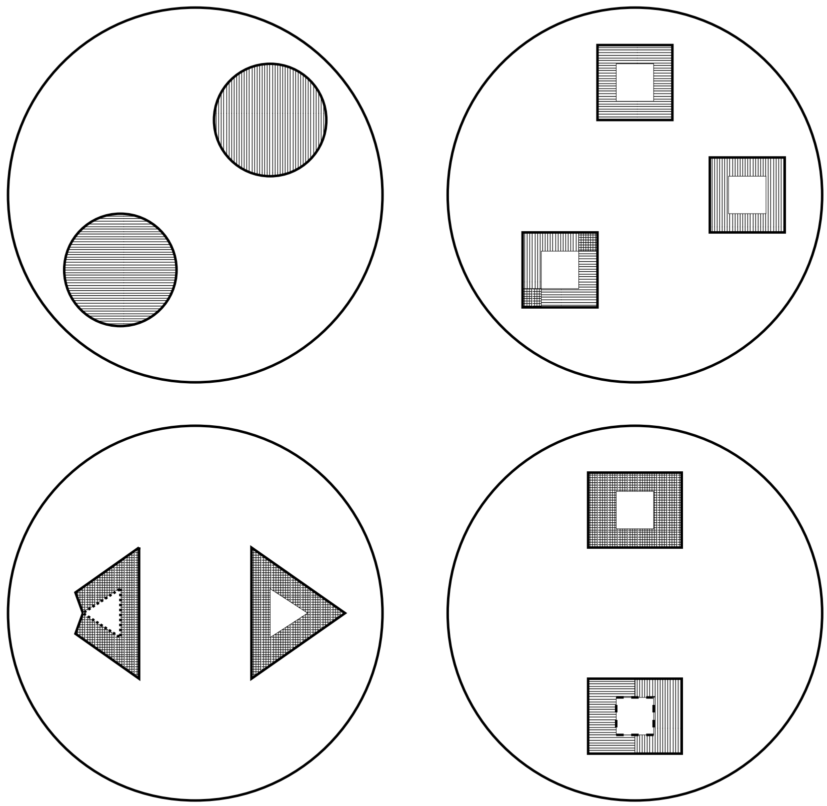

Figure 1. Inclusion geometries of the first four examples. The perturbation κ is strictly positive definite in the regions filled by horizontal lines and zero elsewhere; the perturbation η is strictly positive in the regions filled by vertical lines and zero elsewhere. Top left: Example 2.1. Top right: Example 2.2. Bottom left: Example 2.3. Bottom right: Example 2.4.

and, on the other hand, $\Phi_y|_{\partial\Omega}$ does not belong to the range if y is in the complement of the closure of these squares. In particular, the factorization method identifies the holes as parts of the inhomogeneities. □

Example 2.3. Consider the inclusion geometry of the bottom left image of Figure 1. This time the characterization of Theorem 2.3 is inconclusive since the interior of $\operatorname{supp}_{\partial\Omega}(\kappa, \eta)$ is larger than $\operatorname{sh}(\kappa, \eta)$: The combined $\partial\Omega$-support of κ and η is the union of the two closed polygons marked by the thick solid line whereas the shade of κ and η consists of the interior of the right-hand polygon together with the open region filled by horizontal and vertical lines inside the left-hand polygon. This asymmetry is due to the 'infinite thinness' of the left-hand inclusion at its left-hand edge. As a consequence, Theorem 2.3 does not tell whether $\Phi_y|_{\partial\Omega}$ belongs to the range of $|\Lambda_0 - \Lambda|^{1/2}$ or not if y lies in the unperturbed triangle marked with the thick dashed line. □

Example 2.4. Consider the inhomogeneities in the bottom right image of Figure 1. As in the preceding example, the characterization given by Theorem 2.3 is not conclusive: The combined $\partial\Omega$-support of κ and η is the union of the two closed rectangles marked by the thick solid line whereas the shade of κ and η consists of the interior of the upper rectangle together with the union of the two open regions filled by horizontal and vertical lines, respectively, inside the lower rectangle. This time the mismatch between the interior of $\mathrm{supp}_{\partial\Omega}(\kappa,\eta)$ and $\mathrm{sh}(\kappa,\eta)$ is caused by the vertical line segments that separate the supports of κ and η inside the lower inclusion; the points on these lines do not have neighbourhoods where one of the perturbations is strictly positive. Consequently, Theorem 2.3 does not tell whether $\Phi_y|_{\partial\Omega}$ belongs to the range of $|\Lambda_0-\Lambda|^{1/2}$ or not if y lies on either of these two line segments or in the unperturbed square marked with the thick dashed line. □

Example 2.5. Let D, with $\overline{D}\subset\Omega$, be an arbitrary simply connected and smooth domain. Assume that $\eta=0$ in the whole of Ω and κ is given by

$$\kappa=\begin{pmatrix}1 & 0\\ 0 & 0\end{pmatrix}\quad \text{in } D,\qquad \kappa=0 \quad \text{in } \Omega\setminus\overline{D}.$$

In this case the combined $\partial\Omega$-support of κ and η is $\overline{D}$, but their shade is empty. Consequently, the only thing that Theorem 2.3 tells is that $\Phi_y|_{\partial\Omega}$ does not belong to the range of $|\Lambda_0-\Lambda|^{1/2}$ if $y\in\Omega\setminus\overline{D}$. □

As the above examples indicate, Theorem 2.3 is less unequivocal than earlier results on the factorization method for inverse elliptic boundary value problems (cf. [11, 12, 20]). The reason for this is that earlier papers have not considered inhomogeneities that may have disconnected complements and they have also assumed that the leading order perturbation is positive (or negative) definite in the interior of its support; none of the inclusion geometries of the above examples falls into the framework of the theorems presented in [11, 15, 16, 20]. For inclusions with connected complements, Theorem 2.3 gives almost all earlier results as special cases apart from the following impairment: Theorem 2.3 never tells whether $\Phi_y|_{\partial\Omega}$ is in the range of $|\Lambda_0-\Lambda|^{1/2}$ or not if y belongs to the boundary of the combined $\partial\Omega$-support of κ and η. Usually authors have been able to avoid this uncertainty by assuming that the inclusions, i.e., the supports of the perturbations, have regular boundaries and that the perturbations (or their higher normal derivatives) produce strict jumps of the coefficient functions (or of their higher normal derivatives) at the inclusion boundaries (cf. [6, 11, 15, 16, 17, 20]). Here we assume no regularity of the supports of the L^∞_c-perturbations and only assume that the perturbations are positive (or negative) semidefinite. In particular, the coefficients defined by (4) may be smooth. A related consideration for the inverse conductivity problem with inclusions that have connected complements can be found in [12].

In spite of the above described treatment of inclusions with disconnected complements and the reduced positivity and smoothness assumptions, the most significant improvement that Theorem 2.3 provides to the factorization method for elliptic equations of the type (1) is the following: Earlier papers have either focused on locating the support of κ and treated η, with $\mathrm{supp}\,\eta\subseteq\mathrm{supp}\,\kappa$, as a nuisance causing a compact perturbation that may sometimes result in the failure of the method [11, 15, 20], or they have assumed that $\kappa=0$ and concentrated on locating the support of η [16]. Bearing this history in mind, a remarkable detail about Theorem 2.3 is that it treats κ and η in a symmetric way. In other words, the factorization method finds the interior of the support of η as easily as that of κ even though κ is a higher order perturbation. This observation is supported by the numerical studies presented in Section 3.

2.2. **Proof of the main result.** The proof of Theorem 2.3 is based on the following three lemmas. To begin with, notice that the analog of Lemma 2.3 in [12] yields that the absolute value of the difference of the Neumann-to-Dirichlet maps in Theorem 2.3 is simply the difference itself (for $\kappa, \eta \geq 0$) or minus the difference (for $\kappa, \eta \leq 0$).

Lemma 2.4. *Let Λ_1, Λ_2 and Λ_3 be the Neumann-to-Dirichlet maps corresponding to the coefficient pairs $(\sigma_1, \mu_1), (\sigma_2, \mu_2), (\sigma_3, \mu_3) \in L^\infty(\Omega, \mathbb{R}^{n\times n}) \times L^\infty(\Omega, \mathbb{R})$, respectively. Assume that*

$$\sigma_1 \leq \sigma_2 \leq \sigma_3 \quad \text{and} \quad \mu_1 \leq \mu_2 \leq \mu_3.$$

Then

$$\mathcal{R}\left\{(\Lambda_1 - \Lambda_2)^{1/2}\right\},\ \mathcal{R}\left\{(\Lambda_2 - \Lambda_3)^{1/2}\right\} \subseteq \mathcal{R}\left\{(\Lambda_1 - \Lambda_3)^{1/2}\right\}.$$

Suppose that $\Lambda_2 - \Lambda_3$ is injective. Then $\Lambda_1 - \Lambda_3$ is also injective, and if $f, g \in L^2(\partial\Omega)$ satisfy

$$(\Lambda_2 - \Lambda_3)^{1/2} f = (\Lambda_1 - \Lambda_3)^{1/2} g, \tag{6}$$

then it holds that

$$\|g\|_{L^2(\partial\Omega)} \leq \|f\|_{L^2(\partial\Omega)}.$$

The same assertion remains valid if $\Lambda_2 - \Lambda_3$ is replaced by $\Lambda_1 - \Lambda_2$.

Proof. Reasoning as in the proofs of Lemma 2.3 and 2.4 in [12], it is easy to see that

$$\|(\Lambda_1 - \Lambda_2)^{1/2} f\|_{L^2(\partial\Omega)},\ \|(\Lambda_2 - \Lambda_3)^{1/2} f\|_{L^2(\partial\Omega)} \leq \|(\Lambda_1 - \Lambda_3)^{1/2} f\|_{L^2(\partial\Omega)}, \tag{7}$$

for all $f \in L^2(\partial\Omega)$. In consequence, the claim about the ranges follows by using the same functional analytic argument as in the proof of Lemma 2.4 in [12] (see also [9, Cor. 3.5]).

To prove the second part of the claim, note first that the injectivity of $\Lambda_1 - \Lambda_3$ follows from (7); in particular, both $(\Lambda_1 - \Lambda_3)^{1/2}$ and $(\Lambda_2 - \Lambda_3)^{1/2}$ have dense ranges since they are injective and self-adjoint. Let $f, g \in L^2(\partial\Omega)$ satisfy (6) and estimate as follows:

$$\begin{aligned}
\|g\|_{L^2(\partial\Omega)} &= \sup_{h\in L^2,\, h\neq 0} \frac{\left(g, (\Lambda_1 - \Lambda_3)^{1/2} h\right)_{L^2(\partial\Omega)}}{\|(\Lambda_1 - \Lambda_3)^{1/2} h\|_{L^2(\partial\Omega)}} \\
&= \sup_{h\in L^2,\, h\neq 0} \frac{\left(f, (\Lambda_2 - \Lambda_3)^{1/2} h\right)_{L^2(\partial\Omega)}}{\|(\Lambda_1 - \Lambda_3)^{1/2} h\|_{L^2(\partial\Omega)}} \\
&\leq \sup_{h\in L^2,\, h\neq 0} \frac{\left(f, (\Lambda_2 - \Lambda_3)^{1/2} h\right)_{L^2(\partial\Omega)}}{\|(\Lambda_2 - \Lambda_3)^{1/2} h\|_{L^2(\partial\Omega)}} = \|f\|_{L^2(\partial\Omega)},
\end{aligned}$$

where the inequality follows from (7). Since the claim involving $\Lambda_1 - \Lambda_2$ instead of $\Lambda_2 - \Lambda_3$ can be handled in the same manner, the proof is complete. □

Lemma 2.5. *Let D be a smooth domain such that $\overline{D} \subset \Omega$ and $\Omega \setminus \overline{D}$ is connected and let $A\colon\ L^2(\partial\Omega) \to L^2(\partial\Omega)$ be an injective, bounded, linear operator.*

(a) If $f\colon\ \partial D \to L^2(\partial\Omega)$ is a measurable function with $f(\partial D) \subseteq \mathcal{R}(A)$, then also

$$g : \partial D \to L^2(\partial\Omega), \quad g(z) := A^{-1} f(z) \quad \textit{for all } z \in \partial D$$

is a measurable function.

(b) If

$$\Phi_z|_{\partial\Omega} \in \mathcal{R}(A) \quad \textit{for all } z \in \partial D,$$

and the corresponding preimages are uniformly bounded in $L^2(\partial\Omega)$, then

$$\Phi_y|_{\partial\Omega} \in \mathcal{R}(A) \quad \textit{for all } y \in D.$$

Proof. (a) We start with a standard approximation of f with a sequence of simple functions; cf., e.g., the proof of [7, Sect. II, Thm. 2]. Let $\{v_l\}_{l\in\mathbb{N}}$ be a countable, dense subset of the separable space $L^2(\partial\Omega)$. We define the sets $\tilde\Gamma_{l,m} \subseteq \partial D$, $l, m \in \mathbb{N}$, by

$$\tilde\Gamma_{l,m} := \left\{ z \in \partial D \;\middle|\; \|f(z) - v_l\|_{L^2(\partial\Omega)} < \frac{1}{m} \right\}$$

and for each $M \in \mathbb{N}$ we make a number of these sets disjoint by setting

$$\Gamma_{l,m}^{(M)} := \tilde\Gamma_{l,m} \setminus C_{l,m} \quad \text{for all } l, m \in \mathbb{N},$$

where $C_{l,m}$ is the union of $\tilde\Gamma_{\tilde l,m}$, $\tilde l \in \{l+1, \ldots, M\}$, and $\tilde\Gamma_{\tilde l,\tilde m}$, $\tilde l \in \{1, \ldots, M\}$, $\tilde m \in \{m+1, \ldots, M\}$.

By induction, it follows that the sets $\Gamma_{l,m}^{(M)}$, $l, m \in \{1, \ldots, M\}$, are indeed mutually disjoint. Moreover, for every $z \in \tilde\Gamma_{l,m}$ there exists $\tilde l \in \{1, \ldots, M\}$ and $\tilde m \in \{m, \ldots, M\}$ such that $z \in \Gamma_{\tilde l,\tilde m}^{(M)} \subseteq \tilde\Gamma_{\tilde l,\tilde m}$, which means, in particular, that

$$\left\|f(z) - v_{\tilde l}\right\|_{L^2(\partial\Omega)} < \frac{1}{\tilde m} \le \frac{1}{m}.$$

Denoting by $\chi_{l,m}^{(M)}$ the characteristic functions of $\Gamma_{l,m}^{(M)}$, we define the sequence of simple function $(f_M)_{M\in\mathbb{N}}$,

$$f_M :\ \partial D \to L^2(\partial\Omega), \quad f_M(z) := \sum_{l,m=1}^{M} v_l\, \chi_{l,m}^{(M)}(z).$$

For every $z \in \tilde\Gamma_{l,m}$ and $M \ge \max\{l, m\}$ the above construction yields that

$$\|f_M(z) - f(z)\|_{L^2(\partial\Omega)} < \frac{1}{m}.$$

In particular, we deduce from the denseness of $\{v_l\}_{l\in\mathbb{N}}$ that f_M converges pointwise against f.

Now we define another sequence of simple functions

$$g_M :\ \partial D \to L^2(\partial\Omega), \quad g_M(z) := \sum_{l,m=1}^{M} w_{l,m}\, \chi_{l,m}^{(M)}(z)$$

using the regularized preimages

$$w_{l,m} := (A^*A + m^{-1}I)^{-1}A^*v_l.$$

For every fixed $z \in \partial D$ and sufficiently large M, there exists a unique pair of indices (l, m) such that $z \in \Gamma_{l,m}^{(M)}$. Thus,

$$g_M(z) = (A^*A + \alpha(z, M)I)^{-1}\, A^* f_M(z) \quad \text{with } \alpha(z, M) := \frac{1}{m}.$$

Since $f_M(z) \to f(z)$ and $\|f_M(z) - f(z)\|_{L^2(\partial\Omega)} < \frac{1}{m} = \alpha(z, M)$, it follows from classical results on Tikhonov regularization (cf., e.g., Engl, Hanke and

Neubauer [8, Thm. 5.2]) that g_M converges pointwise towards g as M goes to infinity. Hence, g is measurable.

(b) From the theory of fundamental solutions, it is well-known that the mapping $\partial D \ni z \mapsto \Phi_z|_{\partial\Omega} \in L^2(\partial\Omega)$ is continuous and thus measurable. (This also follows from the explicit representation of $\Phi_z|_{\partial\Omega}$ in Section 3.) Thus, we obtain from (a) that the function $z \mapsto \Psi_z := A^{-1}\Phi_z|_{\partial\Omega}$ is measurable. Since it is also bounded by assumption, it follows that for all $g \in C^\infty(\partial D)$ the $L^2(\partial\Omega)$-valued function $z \mapsto g(z)\Psi_z$ is integrable on ∂D and that

$$\int_{\partial D} g(z)\Phi_z|_{\partial\Omega}\,\mathrm{d}S_z = A\left(\int_{\partial D} g(z)\Psi_z\,\mathrm{d}S_z\right) \in \mathcal{R}(A).$$

Thus, it only remains to show that for every $y \in D$ there exists $g_y \in C^\infty(\partial D)$ such that

$$\Phi_y|_{\partial\Omega} = \int_{\partial D} g_y(z)\Phi_z|_{\partial\Omega}\,\mathrm{d}S_z. \tag{8}$$

To that end, we introduce the Dirichlet-to-Neumann map corresponding to D and the background coefficients (σ_0, μ_0), i.e.,

$$\Lambda_{D,0}^{-1} : h \mapsto \sigma_0 \frac{\partial v}{\partial \nu}\bigg|_{\partial D}, \quad H^{1/2}(\partial D) \to H^{-1/2}(\partial D),$$

where ν is the exterior unit normal of ∂D and $v \in H^1(D)$ is the solution of

$$\sigma_0 \Delta v - \mu_0 v = 0 \quad \text{in } D, \quad v = h \quad \text{on } \partial D.$$

Then we define $g_y \in C^\infty(\partial D)$ by

$$g_y := \sigma_0 \frac{\partial \Phi_y}{\partial \nu}\bigg|_{\partial D} - \Lambda_{D,0}^{-1}(\Phi_y|_{\partial D}).$$

To show that g_y fulfills (8), consider an arbitrary $f \in C^\infty(\partial\Omega)$ and let $u_f \in C^\infty(\overline{\Omega})$ be the corresponding solution of the Neumann boundary value problem (2) with $\sigma = \sigma_0$ and $\mu = \mu_0$. From potential theory it follows that

$$u_f(z) = -\int_{\partial\Omega} f(x)\Phi_z(x)\,\mathrm{d}S_x$$

for all $z \in \Omega$. Thus, using partial integration and the self-adjointness of $\Lambda_{D,0}^{-1}$, we may reason as follows:

$$\begin{aligned}
\int_{\partial\Omega} f(x)\Phi_y(x)\,\mathrm{d}S_x &= \int_{\partial D} \sigma_0 \frac{\partial u_f}{\partial \nu}(z)\,\Phi_y(z)\,\mathrm{d}S_z - \int_{\partial D} \sigma_0 \frac{\partial \Phi_y}{\partial \nu}(z)\,u_f(z)\,\mathrm{d}S_z \\
&= \int_{\partial D} \left(\left(\Lambda_{D,0}^{-1}\Phi_y|_{\partial D}\right)(z) - \sigma_0 \frac{\partial \Phi_y}{\partial \nu}\bigg|_{\partial D}(z)\right) u_f(z)\,\mathrm{d}S_z \\
&= \int_{\partial D} g_y(z) \int_{\partial\Omega} f(x)\Phi_z(x)\,\mathrm{d}S_x\,\mathrm{d}S_z \\
&= \int_{\partial\Omega} f(x) \int_{\partial D} g_y(z)\Phi_z(x)\,\mathrm{d}S_z\,\mathrm{d}S_x.
\end{aligned}$$

Since this holds for every smooth f and $C^\infty(\partial\Omega)$ is dense in $L^2(\partial\Omega)$, the proof is complete.

□

Lemma 2.6. *Let D be as in Lemma 2.5 and let Λ_c be the Neumann-to-Dirichlet map corresponding to the coefficient pair*

$$\sigma_c = \begin{cases} (\sigma_0 + c_1)I & \text{in } D, \\ \sigma_0 I & \text{in } \Omega \setminus \overline{D}, \end{cases} \qquad \mu_c = \begin{cases} \mu_0 + c_2 & \text{in } D, \\ \mu_0 & \text{in } \Omega \setminus \overline{D}, \end{cases}$$

where $c_1 > -\sigma_0$ and $c_2 > -\mu_0$ are real constants. Then $\Phi_y|_{\partial\Omega}$ does not belong to $\mathcal{R}(|\Lambda_0 - \Lambda_c|^{1/2})$ if $y \notin D$.

Furthermore, if either $c_1 = 0$ or $c_2 = 0$, but not both, then $\Lambda_0 - \Lambda_c$ is injective, and there exists $C > 0$ such that for every $y \in D$

$$\Phi_y|_{\partial\Omega} \in \mathcal{R}(|\Lambda_0 - \Lambda_c|^{1/2}) \tag{9}$$

and the preimage $\Psi_y \in L^2(\partial\Omega)$, $|\Lambda_0 - \Lambda_c|^{1/2}\Psi_y = \Phi_y|_{\partial\Omega}$, satisfies

$$\|\Psi_y\|_{L^2(\partial\Omega)} \leq C \left\| \frac{\partial \Phi_y}{\partial \nu} \right\|_{H^{\pm 1/2}(\partial D)}, \tag{10}$$

where the plus sign corresponds to the case $c_1 = 0$, $c_2 \neq 0$ and the minus sign to the case $c_1 \neq 0$, $c_2 = 0$.

Proof. The fact that $\Phi_y|_{\partial\Omega}$ does not belong to $\mathcal{R}(|\Lambda_0 - \Lambda_c|^{1/2})$ if $y \notin D$, as well as the claim about the injectivity of $\Lambda_0 - \Lambda_c$ and the existence of $\Psi_y \in L^2(\partial\Omega)$ in the case $c_1 \neq 0$, $c_2 = 0$, follow straight away from the material in [11, 15]. On the other hand, when $c_1 = 0$ and $c_2 \neq 0$, the injectivity of $\Lambda_0 - \Lambda_c$ and the existence of Ψ_y can be proved by slightly modifying (simplifying) the line of reasoning presented in Section 3 of [16], where an equivalent result is proved for Robin-to-Robin boundary operators. However, since the norm estimate (10) has not been included in earlier papers, we outline here the proof for the case $y \in D$.

To begin with, let us introduce a family of auxiliary operators. For $\phi \in H^s(\partial D)$, $s \geq -1/2$, the boundary value problem

$$\sigma_0 \Delta v - \mu_0 v = 0 \quad \text{in } \Omega \setminus \overline{D}, \quad \sigma_0 \frac{\partial v}{\partial \nu} = 0 \quad \text{on } \partial\Omega, \quad \sigma_0 \frac{\partial v}{\partial \nu} = \phi \quad \text{on } \partial D,$$

has a unique solution $v \in H^1(\Omega \setminus \overline{D})$ that depends continuously on the boundary data. We define the linear, bounded, compact and injective operator $L_s : H^s(\partial D) \to L^2(\partial\Omega)$ by

$$L_s : \phi \mapsto v|_{\partial\Omega},$$

for $s \geq -1/2$.

When $c_1 \neq 0$ and $c_2 = 0$, it follows from the considerations in [11, 20] that the boundary map $|\Lambda_0 - \Lambda_c| : L^2(\partial\Omega) \to L^2(\partial\Omega)$ can be factorized as

$$|\Lambda_0 - \Lambda_c| = L_{-1/2} G_{-1/2} (G_{-1/2})^* (L_{-1/2})^*,$$

where $G_{-1/2} : L^2(\partial D) \to H^{-1/2}(\partial D)$ is an isomorphism. On the other hand, if $c_1 = 0$ and $c_2 \neq 0$, there exists a closely related isomorphism $G_{1/2} : L^2(\partial D) \to H^{1/2}(\partial D)$ such that (cf. [16])

$$|\Lambda_0 - \Lambda_c| = L_{1/2} G_{1/2} (G_{1/2})^* (L_{1/2})^*.$$

As a consequence, $|\Lambda_0 - \Lambda_c|$ is injective, and it follows from fundamental functional analysis (cf., e.g., [11, Lemma 3.5] for an elementary proof) that

$$\mathcal{R}\left\{|\Lambda_0 - \Lambda_c|^{1/2}\right\} = \mathcal{R}(L_{\pm 1/2} G_{\pm 1/2}) = \mathcal{R}(L_{\pm 1/2}),$$

where the plus and minus signs correspond to the cases $c_1 = 0$, $c_2 \neq 0$ and $c_1 \neq 0$, $c_2 = 0$, respectively.

If $y \in D$, it is easy to see that

$$L_{\pm 1/2}\left(\sigma_0 \frac{\partial \Phi_y}{\partial \nu}\bigg|_{\partial D}\right) = \Phi_y|_{\partial\Omega},$$

and so there exists $\Psi_y \in L^2(\partial\Omega)$ that satisfies (9). Moreover, by using the above factorizations and the same argumentation as in the proof of Lemma 2.4, it follows that

$$\|\Psi_y\|_{L^2(\partial\Omega)} = \left\|(G_{\pm 1/2})^{-1}\left(\sigma_0 \frac{\partial \Phi_y}{\partial \nu}\right)\right\|_{L^2(\partial D)} \leq C\left\|\frac{\partial \Phi_y}{\partial \nu}\right\|_{H^{\pm 1/2}(\partial D)},$$

where once again the plus and minus signs correspond to the cases $c_1 = 0$, $c_2 \neq 0$ and $c_1 \neq 0$, $c_2 = 0$, respectively. This completes the proof. □

Then it is the time to provide the proof of Theorem 2.3.

Proof of Theorem 2.3. To begin with, assume that $\kappa, \eta \geq 0$. If $y \in \mathrm{sh}(\kappa, \eta)$, by definition there exists a smooth domain $D \subset \Omega$, with $\overline{D} \subset \Omega$ and $\Omega \setminus \overline{D}$ connected, such that $y \in D$ and for each $\zeta \in \partial D$ there exist constants $\epsilon_\zeta, r_\zeta > 0$ such that

$$\kappa > \epsilon_\zeta I \quad \text{or} \quad \eta > \epsilon_\zeta \quad \text{almost everywhere in } B(\zeta, r_\zeta).$$

Let us introduce an auxiliary function $\iota : \partial D \to \{0, 1\}$ defined by

$$\iota(\zeta) = \begin{cases} 0 & \text{if } \kappa > \epsilon_\zeta I \text{ almost everywhere in } B(\zeta, r_\zeta), \\ 1 & \text{otherwise,} \end{cases}$$

which indicates a perturbation that is strictly positive in a neighbourhood of $\zeta \in \partial D$.

Since ∂D is compact, we may choose a finite set of points $\{\zeta_j\}_{j=1}^m \subset \partial D$ so that

$$\partial D \subset \bigcup_{j=1}^{m} B(\zeta_j, r_j/2), \tag{11}$$

where we have used the shorthand notation $r_j = r_{\zeta_j}$; in the following, we will also write $\epsilon_j = \epsilon_{\zeta_j}$ and $\iota_j = \iota(\zeta_j)$. Let us define a family of auxiliary coefficient pairs $\{\sigma_j, \mu_j\}_{j=1}^m$ by

$$\sigma_j = \begin{cases} \sigma_0 + (1 - \iota_j)\epsilon_j & \text{in } B(\zeta_j, r_j), \\ \sigma_0 & \text{in } \Omega \setminus \overline{B(\zeta_j, r_j)}, \end{cases} \qquad \mu_j = \begin{cases} \mu_0 + \iota_j \epsilon_j & \text{in } B(\zeta_j, r_j), \\ \mu_0 & \text{in } \Omega \setminus \overline{B(\zeta_j, r_j)}, \end{cases}$$

and denote the associated Neumann-to-Dirichlet maps by $\{\Lambda_j\}_{j=1}^m$. According to Lemma 2.6, $\Lambda_0 - \Lambda_j$ is injective and for every $z \in B(\zeta_j, r_j/2)$ there exists $\Theta_{z,j} \in L^2(\partial\Omega)$ such that

$$|\Lambda_0 - \Lambda_j|^{1/2}\Theta_{z,j} = \Phi_z|_{\partial\Omega} \quad \text{and} \quad \|\Theta_{z,j}\|_{L^2(\partial\Omega)} \leq C\left\|\frac{\partial \Phi_z}{\partial \nu}\right\|_{H^{1/2}(\partial B(\zeta_j, r_j))} \leq C_j,$$

where the last inequality is due to the fact that z stays away from the boundary of $B(\zeta_j, r_j)$.

Since $\sigma_0 I \leq \sigma_j I \leq \sigma$ and $\mu_0 \leq \mu_j \leq \mu$, it follows from Lemma 2.4 that $\Lambda_0 - \Lambda$ is injective and that there exists $\Psi_{z,j} \in L^2(\partial\Omega)$ such that

$$|\Lambda_0 - \Lambda|^{1/2}\Psi_{z,j} = \Phi_z|_{\partial\Omega} \quad \text{and} \quad \|\Psi_{z,j}\|_{L^2(\partial\Omega)} \leq C_j \quad \text{for all } z \in B(\zeta_j, r_j/2).$$

Taking advantage of (11) and the injectivity of $|\Lambda_0 - \Lambda|^{1/2}$, it is easy to see that $\Psi_z := \Psi_{z,j}$ is well-defined for all $z \in \partial D$. We have thus constructed $\{\Psi_z\}_{z \in \partial D} \subset L^2(\partial\Omega)$ such that $|\Lambda_0 - \Lambda|^{1/2}\Psi_z = \Phi_z|_{\partial\Omega}$ for all $z \in \partial D$ and

$$\sup_{z \in \partial D} \|\Psi_z\|_{L^2(\partial\Omega)} \leq \max_{j=1,\ldots,m} C_j < \infty.$$

As a consequence, Lemma 2.5 shows that $\Phi_y|_{\partial\Omega}$ belongs to the range of $|\Lambda_0 - \Lambda|^{1/2}$.

Continue assuming that $\kappa, \eta \geq 0$ and let now $y \in \Omega \setminus \operatorname{supp}_{\partial\Omega}(\kappa, \eta)$. Since κ and η are compactly supported, it follows from the definition of the combined $\partial\Omega$-support that there exists a smooth domain D_y such that $y \notin D_y$, $\operatorname{supp}_{\partial\Omega}(\kappa, \eta) \subset D_y$, $\overline{D}_y \subset \Omega$ and $\Omega \setminus \overline{D}_y$ is connected. We define yet another pair of auxiliary coefficients by

$$\sigma_y = \begin{cases} \sigma_0 + c_1 & \text{in } D_y, \\ \sigma_0 & \text{in } \Omega \setminus \overline{D}_y, \end{cases} \qquad \mu_y = \begin{cases} \mu_0 + c_2 & \text{in } D_y, \\ \mu_0 & \text{in } \Omega \setminus \overline{D}_y, \end{cases}$$

where the scalar constants $c_1, c_2 \geq 0$ are chosen so that $\sigma_y I > \sigma$ and $\mu_y > \mu$ almost everywhere in Ω. Now Lemmas 2.4 and 2.6 tell us that

$$\Phi_y|_{\partial\Omega} \notin \mathcal{R}\left\{|\Lambda_0 - \Lambda_y|^{1/2}\right\} \supseteq \mathcal{R}\left\{|\Lambda_0 - \Lambda|^{1/2}\right\},$$

where Λ_y is the Neumann-to-Dirichlet map corresponding to the pair (σ_y, μ_y). This proves the claim for $\kappa, \eta \geq 0$.

Since the case that $\kappa, \eta \leq 0$ can be handled in exactly the same way, the proof is complete. □

3. Numerical experiments.

3. Numerical experiments. We will now present some numerical experiments to verify and illustrate our theoretical findings. In all cases, Ω is the two-dimensional unit disk and the background diffusion and absorption coefficients are chosen to be $\sigma_0 = 0.05$ and $\mu_0 = 0.5$, which correspond to the optical parameters of a neonatal head of radius 25 mm, cf. [1, 18].

The numerical simulation of the Neumann-to-Dirichlet boundary maps is done in the same way as in [12]: On the boundary $\partial\Omega$ we apply the L^2-orthonormal basis functions

$$\mathcal{B} := \left\{ \frac{1}{\sqrt{2\pi}}, \frac{1}{\sqrt{\pi}}\sin(k\phi), \frac{1}{\sqrt{\pi}}\cos(k\phi) \;\middle|\; k = 1, \ldots, 128 \right\}$$

as inputs. Here and in the following, the pair (r, ϕ) denotes the polar coordinates with respect to the center of Ω. For given perturbations κ and η, let $u \in H^1(\Omega)$ be the solution of (2) with $\sigma = \sigma_0 + \kappa$, $\mu = \mu_0 + \eta$, and let $u_0 \in H^1(\Omega)$ be the corresponding solution for the unperturbed background coefficients σ_0 and μ_0.

For every $f \in \mathcal{B}$ we compute the difference $v := u_0 - u \in H^1(\Omega)$ with the commercial finite element software Comsol by solving the variational problem

$$\int_\Omega (\sigma \nabla v \cdot \nabla w + \mu v w)\, \mathrm{d}x = \int_\Omega (\kappa \nabla u_0 \cdot \nabla w + \eta u_0 w)\, \mathrm{d}x \quad \text{for all } w \in H^1(\Omega),$$

which is obtained by subtracting the variational equations for u and u_0. Since κ and η are compactly supported in Ω, this is equivalent to

$$\nabla \cdot \sigma \nabla v - \mu v = \nabla \cdot \kappa \nabla u_0 - \eta u_0$$

with the homogeneous Neumann boundary condition on $\partial\Omega$. On the right hand side we use the exact solutions u_0 for the aforementioned input functions f, i.e.,

$$\frac{c_0}{\sqrt{2\pi}} I_0\left(\sqrt{\frac{\mu_0}{\sigma_0}} r\right), \quad \frac{c_k}{\sqrt{\pi}}\cos(k\phi) I_k\left(\sqrt{\frac{\mu_0}{\sigma_0}} r\right), \quad \text{and} \quad \frac{c_k}{\sqrt{\pi}}\sin(k\phi) I_k\left(\sqrt{\frac{\mu_0}{\sigma_0}} r\right),$$

where

$$c_k := \frac{2}{\sqrt{\mu_0\sigma_0}\left(I_{k-1}\left(\sqrt{\frac{\mu_0}{\sigma_0}}\right) + I_{k+1}\left(\sqrt{\frac{\mu_0}{\sigma_0}}\right)\right)}, \quad k = 0, \ldots, 128,$$

and I_α, $\alpha \in \mathbb{Z}$, are the *modified Bessel functions of the first kind* (cf. [18]). As the difference of u and u_0 is considerably smaller than u and u_0, this approach leads to a higher precision than computing u and u_0 separately. The boundary data $v|_{\partial\Omega} = (u_0 - u)|_{\partial\Omega}$ is then expanded in the orthonormal basis $\mathcal{B}$, so that we obtain a discrete approximation $M \in \mathbb{R}^{257\times 257}$ of the operator $\Lambda_0 - \Lambda$.

We turn next to the computation of the singular function Φ_y, i.e., the solution of (5). Let K_0 be the zeroth order *modified Bessel function of the second kind*. Then,

$$h_y(x) := -\frac{1}{2\pi\sigma_0} K_0\left(\sqrt{\frac{\mu_0}{\sigma_0}}\; |y-x|\right)$$

satisfies the first part of (5) and thus differs from Φ_y only by a homogeneous solution. Hence, it follows that

$$\Phi_y|_{\partial\Omega} = h_y|_{\partial\Omega} - \Lambda_0\left(\sigma_0 \frac{\partial h_y}{\partial\nu}\bigg|_{\partial\Omega}\right).$$

The operator Λ_0 is diagonalized by the orthonormal basis $\mathcal{B}$ and its eigenvalues are easily computed from the exact solutions given above. Thus, we obtain the expansion $\tilde{\Phi}_y \in \mathbb{R}^{257}$ of $\Phi_y|_{\partial\Omega}$ in the basis $\mathcal{B}$ in a straightforward manner by using the corresponding expansions of $h_y|_{\partial B}$ and $\sigma_0 \frac{\partial h_y}{\partial \nu}$ (cf. [18]).

For the numerical implementation of the range test

$$\Phi_y|_{\partial\Omega} \in \mathcal{R}(|\Lambda_0 - \Lambda|^{1/2}), \tag{12}$$

we proceed as in [12]. Let

$$(\Lambda_0 - \Lambda)v_j = \lambda_j v_j, \qquad j \in \mathbb{N},$$

be a spectral decomposition of the compact, self-adjoint, and injective operator $\Lambda_0 - \Lambda$ with orthonormal basis of eigenfunctions $\{v_j\} \subset L^2(\partial\Omega)$ and eigenvalues $\{\lambda_j\} \subset \mathbb{R}$ (sorted in decreasing order of absolute value). The Picard criterion yields that (12) holds if and only if

$$f(y) := \frac{1}{\|\Phi_y|_{\partial\Omega}\|^2_{L^2(\partial\Omega)}} \sum_{j=1}^{\infty} \frac{|\langle \Phi_y|_{\partial\Omega}, v_j\rangle_{L^2(\partial\Omega)}|^2}{|\lambda_j|} < \infty.$$

Using a singular value decomposition of the discrete approximation $M \in \mathbb{R}^{257\times 257}$,

$$M\tilde{v}_j = \tilde{\lambda}_j \tilde{u}_j, \qquad M^*\tilde{u}_j = \tilde{\lambda}_j \tilde{v}_j, \qquad j = 1,\ldots,257,$$

with nonnegative $\{\tilde{\lambda}_j\} \subset \mathbb{R}$ (sorted in decreasing order) and orthonormal bases $\{\tilde{u}_j\}, \{\tilde{v}_j\} \subset \mathbb{R}^{257}$, we approximate the function $f(y)$ by

$$\tilde{f}(y) := \sum_{j=1}^{m} \frac{(\tilde{\Phi}_y \cdot \tilde{v}_j)^2}{|\tilde{\lambda}_j|} \Big/ \sum_{j=1}^{m} (\tilde{\Phi}_y \cdot \tilde{v}_j)^2,$$

where m is chosen so that $\tilde{\lambda}_{m+1}$ is the first singular value below the expected measurement error.

To obtain a numerical criterion for deciding if the infinite sum $f(y)$ attains the value ∞ from the mere knowledge of the approximate value $\tilde{f}(y)$, which is always finite, a threshold $C_\infty > 0$ is needed to distinguish the points with *large* values $\tilde{f}(y) \geq C_\infty$ from those with *small* values $\tilde{f}(y) < C_\infty$. A reconstruction of a set containing information on the combined $\partial\Omega$-support of κ and η (see Theorem 2.3) is then obtained by evaluating $\tilde{f}(y)$ on a grid of points $\{y_n\} \subset \Omega$ and saying that all points with $\tilde{f}(y_n) < C_\infty$ belong to this set of interest. Choosing different threshold

First published in Inverse Problems and Imaging in Vol. 2, No. 3, 2008,
published by the American Institute of Mathematical Sciences

values C_∞ corresponds to choosing different level contours of $\tilde{f}(y)$ or, equivalently, of a monotone function of $\tilde{f}(y)$.

In our numerical experiments, we plot the indicator function

$$\operatorname{Ind}(y) := \left(\log \tilde{f}(y)\right)^{-1} \tag{13}$$

on an equidistant grid $\{y_n\} \subset \Omega$, which is chosen independently of the finite element mesh that is used for solving the forward problems. We also show the level contour that fits best to the true $\partial\Omega$-support (chosen by hand on a purely subjective basis). In practice, the choice of the threshold requires additional information, e.g., from previous experiments, and there is no guarantee that an optimal contour is found. To illustrate the sensitivity of our reconstructions with respect to the threshold, we also plot the level contours $\operatorname{Ind}^{-1}(C_\infty)$ for $C_\infty = 0.9 \cdot \hat{C}_\infty$ and $C_\infty = 1.1 \cdot \hat{C}_\infty$, where $\hat{C}_\infty$ is the threshold corresponding to the optimal level contour.

Figure 2 illustrates the reconstructions that we obtained using exact simulated data. The supports of the perturbations η, κ are the sets from Examples 2.1–4. On their respective supports we set $\eta = \mu_0$ and $\kappa = \sigma_0$, i.e., the perturbed coefficients are twice as high as the background coefficients. The left column of Figure 2 shows the graph of the indicator function defined by (13) using all singular values above machine precision level. The edges of the supports of η and κ are plotted by a dashed, light cyan line. For distinguishing the respective supports we refer to Figure 1. As explained above, the second column of Figure 2 shows the corresponding level curves for the optimal threshold $\hat{C}_\infty$ (light solid red line), and for the two perturbed thresholds $0.9 \cdot \hat{C}_\infty$ (outer dotted green line) and $1.1 \cdot \hat{C}_\infty$ (inner dotted green line). The true inclusions are marked with a dashed black line.

As Figure 2 demonstrates, the factorization method provides a relatively good reconstruction of the combined $\partial\Omega$-support of κ and η if exact data is available. In particular, the algorithm locates simultaneously both diffuse and absorbing inclusions, although the behaviour of the indicator function depends somewhat on the type of the inhomogeneity in question: Ind tends to have a broad and low elevation over the support of κ whereas there is a more concentrated and higher peak over the support of η. Experiments with other parameter values, however, reveal that the relative heights of the humps in the graph of Ind depend strongly on the choice of σ_0 and μ_0 as well as on the strengths of the perturbations κ and η. An interesting detail in Figure 2 is that the difference between $\operatorname{supp}_{\partial\Omega}(\kappa, \eta)$ and $\operatorname{sh}(\kappa, \eta)$ in the latter two experiments (see Examples 2.3 and 2.4, and Theorem 2.3) does not seem to affect the reconstructions very much: The method seems to provide an approximation of the combined $\partial\Omega$-support of κ and η also in these cases.

Let us remark that our unperturbed simulated data is of course not really exact but contains all kinds of discretization errors. Using the magnitude of the nonsymmetric part of M as in [10], we estimated the relative error in the spectral norm to be around $2 \cdot 10^{-6}$ for our four examples. However, this error is of a systematic nature, which we observed to have a lesser impact on the reconstructions than random errors do.

In addition to using the unperturbed simulated measurement matrix M, we therefore also test the method after adding 0.1% random noise to M. More precisely, we generate a random matrix $E \in \mathbb{R}^{257 \times 257}$ with uniformly distributed entries between -1 and 1. Then E is scaled to the noise level with respect to its spectral

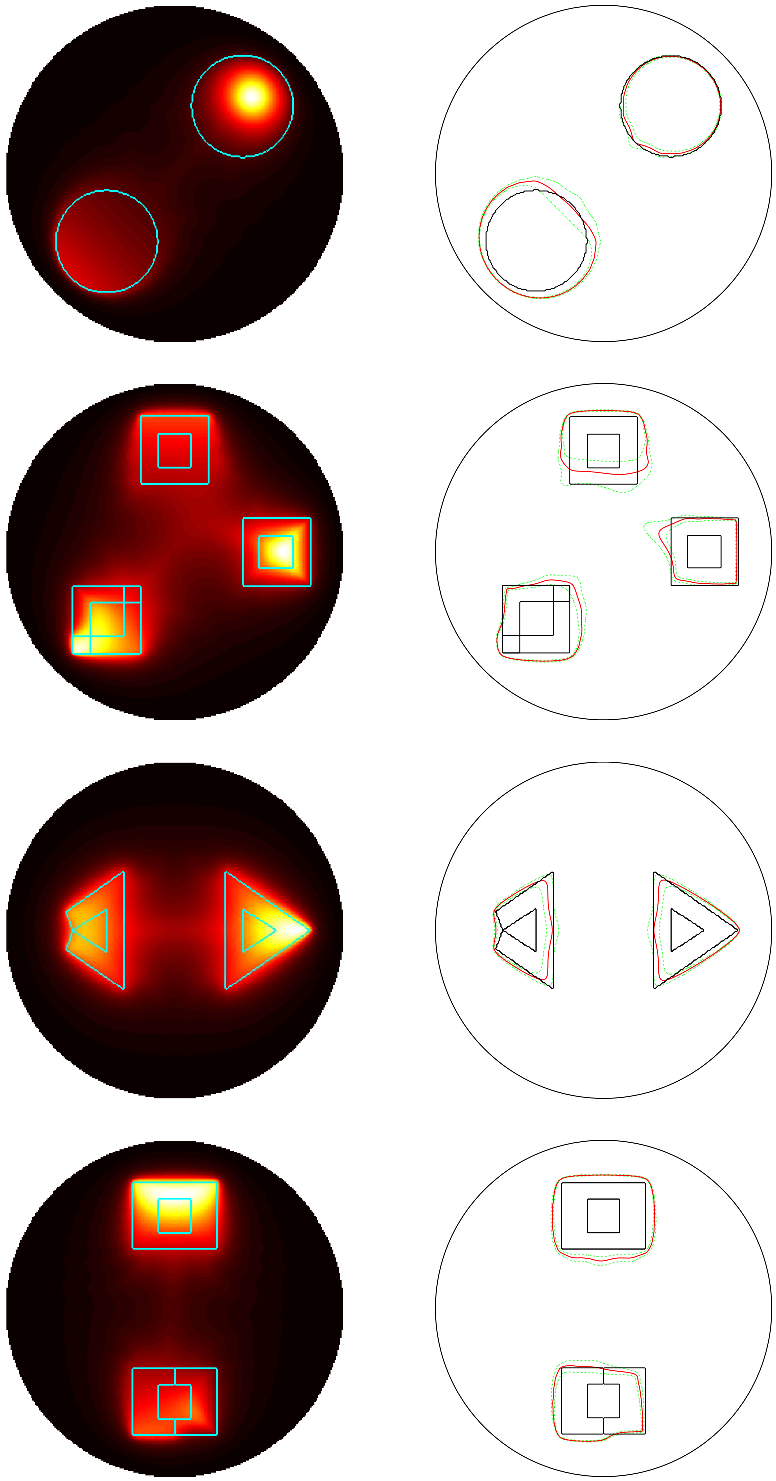

Figure 2. Numerical reconstructions with exact data.

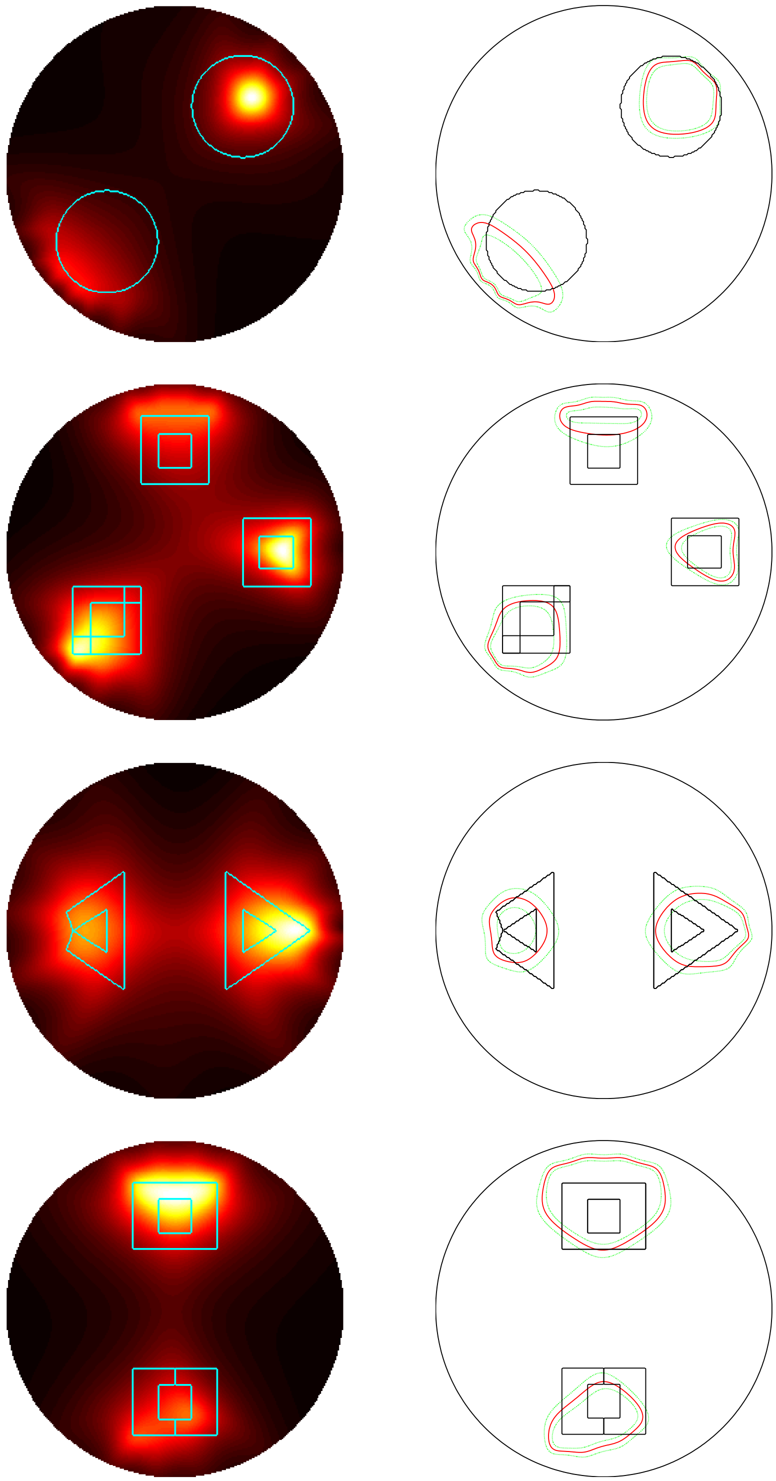

FIGURE 3. Numerical reconstructions with noisy data.

First published in Inverse Problems and Imaging in Vol. 2, No. 3, 2008,
published by the American Institute of Mathematical Sciences

norm $\|E\|_2$ and added to M, i.e., we replace M with

$$M_\epsilon := M + 10^{-3}\,\|M\|_2\,\frac{E}{\|E\|_2}.$$

Accordingly, only singular values larger than $10^{-3}\,\|M_\epsilon\|$ are now used in the truncated Picard series in the definition of $\tilde{f}(y)$.

Figure 3, which is organized in the same way as Figure 2, illustrates the reconstructions corresponding to noisy simulated data. As expected, the reconstructions are more blurred than in the noiseless case and one cannot make out the exact shapes of the inhomogeneities based on the graphs of the indicator functions. However, the images in Figure 3 still provide useful informations on the approximate locations of the inclusions. The effect that the measurement noise has on the quality of the reconstructions is in line with the observations in [5, 13, 12], where similar experiments are presented in the framework of electrical impedance tomography.

4. Conclusions.

We have shown that in the framework of coercive elliptic partial differential equations of the divergence type the factorization method locates simultaneously the supports of positive (or negative) perturbations of the leading and zeroth order coefficients. Furthermore, we have demonstrated that the method remains functional even if the inhomogeneities have irregular boundaries and disconnected complements. Numerical experiments with simulated data confirm our theoretical results.

Acknowledgements. This work was conducted while the first author was employed at the Johann Radon Institute for Computational and Applied Mathematics (RICAM), Austrian Academy of Sciences, Altenbergerstr. 69, A-4040 Linz, Austria.

The work of the second author was supported by the Academy of Finland (project 115013), the Finnish Funding Agency for Technology and Innovation (project 40084/06), the Finnish Cultural Foundation, and the Finnish Foundation for Technology Promotion.

REFERENCES

[1] S. R. Arridge, *Optical tomography in medical imaging*, Inverse Problems, **15** (1999), R41–R93.

[2] S. R. Arridge and W. R. B. Lionheart, *Nonuniqueness in diffusion-based optical tomography*, Opt. Lett., **23** (1998), 882–884.

[3] K. Astala and L. Päivärinta, *Calderon's inverse conductivity problem in the plane*, Ann. of Math., **163** (2006), 265–299.

[4] G. Bal, *Reconstructions in impedance and optical tomography with singular interfaces*, Inverse Problems, **21** (2005), 113–131.

[5] M. Brühl and M. Hanke, *Numerical implementation of two noniterative methods for locating inclusions by impedance tomography*, Inverse Problems, **16** (2000), 1029–1042.

[6] M. Brühl, *Explicit characterization of inclusions in electrical impedance tomography*, SIAM J. Math. Anal., **32** (2001), 1327–1341.

[7] J. Diestel and J. J. Uhl, "Vector Measures," vol. **15** of Mathematical Surveys, American Mathematical Society, Providence, Rhode Island, 1977.

[8] H. W. Engl, M. Hanke and A. Neubauer, "Regularization of Inverse Problems," vol. **375** of Mathematics and Its Applications, Kluwer Academic Publishers, Dordrecht, 1996.

[9] F. Frühauf, B. Gebauer and O. Scherzer, *Detecting interfaces in a parabolic-elliptic problem from surface measurements*, SIAM J. Numer. Anal., **45** (2007), 810–836.

[10] B. Gebauer, M. Hanke, A. Kirsch, W. Muniz and C. Schneider, *A sampling method for detecting buried objects using electromagnetic scattering*, Inverse Problems, **21** (2005), 2035–2050.

[11] B. Gebauer, *The factorization method for real elliptic problems*, Z. Anal. Anwend., **25** (2006), 81–102.

[12] B. Gebauer and N. Hyvönen, *Factorization method and irregular inclusions in electrical impedance tomography*, Inverse Problems, **23** (2007), 2159–2170.

[13] M. Hanke and M. Brühl, *Recent progress in electrical impedance tomography*, Inverse Problems, **19** (2003), S65–S90.

[14] J. Heino and E. Somersalo, *Estimation of optical absorption in anisotropic background*, Inverse Problems, **18** (2002), 559–573.

[15] N. Hyvönen, *Characterizing inclusions in optical tomography*, Inverse Problems, **20** (2004), 737–751.

[16] N. Hyvönen, *Application of a weaker formulation of the factorization method to the characterization of absorbing inclusions in optical tomography*, Inverse Problems, **21** (2005), 1331–1343.

[17] N. Hyvönen, *Application of the factorization method to the characterization of weak inclusions in electrical impedance tomography*, Adv. in Appl. Math., **39** (2007), 197–221.

[18] N. Hyvönen, *Locating transparent regions in optical absorption and scattering tomography*, SIAM J. Appl. Math., **67** (2007), 1101–1123.

[19] A. Kirsch, *Characterization of the shape of a scattering obstacle using the spectral data of the far field operator*, Inverse Problems, **14** (1998), 1489–1512.

[20] A. Kirsch, *The factorization method for a class of inverse elliptic problems*, Math. Nachr., **278** (2005), 258–277.

[21] S. Kusiak and J. Sylvester, *The scattering support*, Comm. Pure Appl. Math., **56** (2003), 1525–1548.

[22] A. I. Nachman, *Global uniqueness for a two-dimensional inverse boundary value problem*, Ann. of Math., **143** (1996), 71–96.

[23] J. Sylvester and G. Uhlmann, *A global uniqueness theorem for an inverse boundary value problem*, Ann. of Math., **125** (1987), 153–169.

Received December 2007; revised June 2008.

E-mail address: gebauer@math.uni-mainz.de
E-mail address: nuutti.hyvonen@hut.fi